Parameters for drilling a stepped microhole of nitride ceramics using Taguchi-based grey relational analysis method

Dar-Yuan Chang (zdy4@ulivey.pccu.edu.tw)
Chinese Culture University https://orcid.org/0000-0003-2298-8147
Chien-Hung Lin
Hsiang-Cheng Chien

Research Article

Keywords: Microdrilling, Nitride ceramics, Thrust, Taguchi's method, Factorial interactivity, Grey Relational Analysis

Posted Date: May 11th, 2022

DOI: https://doi.org/10.21203/rs.3.rs-1566188/v1

Abstract

Microdrilling is an essential process in the semiconductor industry to produce microholes for wafer testing instruments such as a wafer probe card. The microholes are laid on an insulating ceramic plate in an array form for piloting microprobes to their specified positions, which are commonly machined by a peck-drilling process. This study investigated the parameters of cutting speed, feed rate, and depth in the peck-drilling process for making a stepped microhole of nitride ceramic plates. A two-level microdrilling experiment was first carried out to investigate the thrust force in drilling a 310-μm-diameter through microhole for checking the interactivity between the drilling parameters. After clarifying parametric interactions, Taguchi's three-level fractional-factorial experiment of a stepped microhole was performed to derive "preferred factorial level set" for minimizing the thrust force and improving hole characteristics. Furthermore, Grey Relational Analysis (GRA) model was built to infer "optimal parameters level design" for considering the multi-characteristic problem of the microhole drilled. Experimental validations were implemented to confirm the analytical results. Experimental data provide useful references for drilling a stepped microhole of nitride ceramic plates.

1. Introduction

As the trend of miniaturized products, micromachining is a key technique to satisfy functional requirements in various precision industries including automobile, aerospace, electronics, medical implants, biomedicine, robotics, and so on [1]. Microdrilling is become more prominently for fabricating microholes in electronics and computer industries such as printed circuit boards, integrated circuitry masking [2], and the wafer testing components discussed in this study. The processes must be closely controlled to produce microholes with accurate dimensions, good straightness, small roundness and positional errors, and lengthen tool life.

Mechanical drilling using a microdrill is a cost-efficient method for making microholes in a miniature part [1]. However, some difficulties have to be overcome; for example, a large load cannot be put on the microdrill due to its low strength and rigidity. In addition, owing to the smaller drill flutes, removal of the drilled chips is easy to be obstructed [3]. **Hyacinth Suganthi et al.** [2] indicated main factors affecting the size and position of the microholes including the process of microdrilling, tools, speeds and feeds, parallelism, vibration and sound, and positional repeatability. Several researchers have presented their experiences in mechanical microdrilling described as follows.

Cutting force is the principal issue on the drilling by a microdrill. **Patra et al.** [4] indicated that downscaling of the conventional drill to a microdrill increases the aspect ratio of the tool and affects the thrust force and radial components. Increasing in the axial cutting force causes the drill bending due to the low stiffness. **Anand et al.** [5] presented a force model for the mechanistic microdrilling with considerations of tool edge radius and minimum chip thickness. **Kim et al.** [6] developed a tool monitoring system for detecting the thrust force in peck-drilling cycles to improve microdrill life. The thrust force detected was below 3 N in drilling a 250-μm-diameter hole of a plain carbon steel (AISI 1045). **Anand** and **Patra** [7] performed microdrilling experiments of carbon fiber reinforced plastic (**CFRP**) to investigate the effects of feed and cutting speed on the cutting force components and hole quality. The thrust force was about 4 N in drilling a 0.5-mm-diameter hole. **Rahamathullah** and **Shunmugam** [8] investigated the thrust force in drilling a 320-μm-diameter microhole of carbon fabric laminate composites. The thrust force increases with an increase in feed and a decrease in spindle speed. Actual thrust forces detected were from 2 to 3.8 N.

Run out is one of common and undesired phenomenon in the drilling process. It causes tool breakage, surface damage, or dimensional inaccuracy. **Beruvides et al.** [9] believed that run out consists in an eccentric motion of the drill generated by the excessive centrifugal force. Drilling by a high aspect ratio drill needs to be checked carefully. **Endo** and **Marui** [3] said rotational cutting speed is almost zero near the chisel point in the small-hole drilling. At that point, the drill only has a small axial velocity corresponding to the feed motion. Accordingly, the run out easily occurs owing to the small error in the drill size. **Chang** and **Lin** [10] made a center-pilot hole first in the microdrilling process by a short-body drill, to reduce the probability of run out in the inlet stage. Size characteristics of the holes drilled can be controlled effectively. **Wang et al.** [11] analyzed the effect of pilot hole in the drilling of CFRP composites. In the drilling of a 4-mm hole assisted by a 1-mm pilot hole, the thrust force was reduced by approximately 55% compared to the none-pilot drilling.

Most literature showed that both cutting speed and feed rate are the principal parameters affecting the cutting force and hole characteristics. **Aysal** [12] used Taguchi's experiment and analysis of variance (**ANOVA**) method to investigate the effects of drilling parameters (cutting speed, feeds, point angle of the drill) on surface roughness and burr in the drilling of carbon black reinforced polyethylene. **Rajmohan** and **Palanikumar** [13] optimized machining parameters (spindle speed, feed, drill type) in the drilling of hybrid metal matrix composites by Taguchi's L_9 orthogonal array (**OA**) experiment. The characteristics examined included the thrust force, surface roughness, and torque. **Shunmugesh** and **Panneerselvam** [14] performed microdrilling experiments of CFRP to discuss the parameters of spindle speed, feed rate, and drill diameter by Taguchi's L_{27} OA to derive optimum conditions for reducing the delamination factor, circularity, and cylindricity simultaneously. **Thanikasalam et al.** [15] developed an online tool-conditions monitoring system to investigate process parameters for surface integrity and hole quality in deep hole drilling of AISI 1045 carbon steel. The control factors in L_9 OA were the spindle speed, feed rate, and coolant pressure. **Ravisubramanian** and **Shunmugam** [16] analyzed the thrust force and torque in the drilling of 6061-T6 aluminum alloy by a 0.5-mm-diameter drill. They compared the thrust force and torque in peck-drilling and direct drilling. A maximum reduction of 52% in thrust force was found.

Applications of ceramic plates with microfeatures are widespread uses for electronic accessories, electrical components, thermal equipment, and catalytic converters [1]. However, the machinability of ceramics is poor due to its brittle behavior and high hardness. To develop an efficient process of ceramic microdrilling is important for controlling the hole's precision, reducing manufacturing cost, and maximizing productivity. Some researchers devote to the use of ultrasonic vibration-assisted mechanism to overcome the problems of exit chipping and tool wear in the drilling of ceramics [17–19]. Cutting force can be decreased due to dynamic friction and aerodynamic lubrication from the periodical vibration, and obtain better cutting performance [17]. According to

the fracture mechanism of drilling engineering ceramics, in the terminal period of drilling, the stress on the periphery of the hole exit is at its maximum and causes a fracture [18]. **Liu et al.** [19] used a rotary ultrasonic spindle system to reduce the microchipping or cracking at the exit in drilling of alumina oxide ceramics. The tool wear was decreased. Nevertheless, few studies published are focused on the mechanical microdrilling of ceramics. In our previous study [20], a two-segment peck-drilling process was proposed to fabricate a 55-μm-diameter microhole. The variation of hole diameter can be controlled within 0.67 μm.

As the literatures mentioned above, the machining characteristics in microdrilling mostly discussed are cutting force [4–9, 11, 13, 16, 17, 21–22] and torque [8, 11, 13, 16]; the hole characteristics include dimensional accuracy [3, 8, 10, 17, 20], circularity or roundness [7–8, 10, 14–15, 20–21], burrs and roughness of hole wall [12–13, 15], and tool wear [15, 19–20]. This is a complicated multi-characteristic problem.

Grey Relational Analysis **(GRA)** is one of methods widely used to optimize manufacturing process that considers several input factors and multiple responses simultaneously. Some GRA models have been presented to infer the optimal parameters design in mechanical drilling processes. **Rajmohan** and **Palanikumar** [13] applied GRA method to optimize machining parameters in the drilling of hybrid metal matrix composites based on the L_9 OA experimental data. The characteristics considered including the thrust force, surface roughness, and torque. **Shunmugesh** and **Panneerselvam** [14] performed the multi-characteristic analysis in the drilling of CFRP. Data of L_{27} OA experiment were used as the inputs to GRA model for minimizing the delamination factor, circularity, and cylindricity. **Thanikasalam et al.** [15] optimized the multi-objective problem of the deep drilling process of a mild steel (AISI 1045) by coupling Taguchi's L_9 OA data and GRA method. Six characteristics were considered such as surface roughness, circularity, cylindricity, hole wall temperature, tool wear, and material removal rate (**MRR**). **Yaşar et al.** [21] presented the use of Taguchi-based GRA method to optimize the machinability characteristics of thrust force and roughness in the drilling of a polypropylene composite based on L_{27} OA data.

For the experiments on mechanical drilling, several studies [4, 7, 9, 17] analyzed both principal parameters of cutting speed and feed rate by the three-level L_9 OA. Nine sets of full-factorial experiments were performed to evaluate the factorial effects on the characteristics examined and derived "preferred factorial level set". Some literatures [10, 13, 15, 18, 21] added one or two parameters in their experiment, and analyzed them by Taguchi's fractional-factorial OA such as L_9, L_{16}, L_{18}, and L_{27}. Afterward, experimental validations were implemented to confirm the analytical results. Moreover, several researchers [5, 8, 12, 14, 16, 19] increased the number of factorial levels to derive the "optimal factorial level set" by a full-factorial experiment directly. However, when the replicated trials are included, the experimental scale and expense are always huge.

Although Taguchi's OAs possess orthogonal properties, the interactivities between control parameters/factors are not checked in most study. Experimental errors due to the unknown or uncontrolled factors may affect analytical results [23]. Therefore, interactions between the control factors are suggested to be discussing here, especially in developing a new process.

This study investigated the microdrilling process of a nitride ceramic plate of machining a stepped microhole matched with a spring-loaded needle used in the wafer testing industry. A two-level OA experiment (L_8) of a through microhole was first carried out to check the interactions between the peck-drilling parameters analyzed. After interactivity discussion, a three-level OA experiment (L_9) of making a stepped microhole was performed to derive the "preferred factorial level set" for minimizing the thrust force and improving the hole characteristics. Furthermore, a Taguchi-based GRA model was built to solve the multi-characteristic problem considering the accuracies of hole diameter, roundness, and positional error simultaneously. Final, the analytical results were showed by experimental validations.

2. Materials And Experimentation

2.1 Mechanical microdrilling process

Twist drills can be used to drill a hole with 50-μm diameter or larger only. Using proper drilling conditions, metals, plastics, and composites could be proceed effectively and obtain satisfied quality [2]. In the drilling of hard-brittle ceramic materials, discontinuous chips are generated. When a high-aspect ratio drill is used in microdrilling, chips are often obstructed in drill flutes that result in the increasing of machining resistance and cause the drill bending or breakage. Peck-drilling cycle can eliminate the chip clogging, decrease the thrust force, lower the temperature in cutting zone, and provide a better surface finish [22].

In this study, experimental microholes were machined by the peck-drilling cycle applied with air-cooling continuously. The target diameter was 310 μm. To avoid the drill walking on workpiece surface at the beginning, a center-pilot hole of 300-μm diameter was first drilled by a high stiffness drill. The length of drill body was only 0.15 mm, and the depth of pilot hole was specified at 5% of the plate thickness, 0.06 mm. Subsequently, the main hole body was drilled by a 310-μm-diameter microdrill. Figure 1 shows the tungsten carbide twist drills used, made by Sphinx Tools Ltd, Swiss. The point angle was 118 degrees.

This study investigated three peck-drilling parameters of cutting speed, feed rate, and depth of peck-drilling, specified as control factors in Taguchi's OA experiment. Figure 2 shows the tool motions in the peck-drilling cycles. The retreating point was set at 0.2 mm above the workpiece surface. The depth of peck-drilling (**J**) was designated as a control factor and the retreating distance (**d**) was 0.02 mm constantly.

2.2 Experimental material and specimens

A machinable nitride ceramic, Photoveel II, was experimented in this study. The material properties are listed in Table 1. Figure 3 shows an experimental ceramic plate which contains five drilling zones. Ten pin holes of 2-mm diameter were drilled in advance for locating the drilling zone in operations. The thickness of this plate was 1.27 mm. Figure 4**(a)** shows the cross section of the stepped microhole discussed. The diameter of the upper main hole was

310 μm with a depth of 1.1 mm, and the diameter of the bottom through hole was 156 μm. Figure 4**(b)** shows the spring-loaded needle matched to the stepped hole used in wafer testing. Diameter of the needle pin is 0.14 ± 0.01 mm.

Table 1. Properties of the machinable nitride ceramic—Photoveel II

Physical and mechanical		Thermal properties	
Density (g/cm^3)	2.56	Operating temperature (°C)	1000
Bending strength (MPa)	440	Coeff. of thermal expansion ($1/°C \times 10^{-6}$)	1.4(RT ~ 400°C)
Vickers hardness (GPa)	2.3	Coeff. of thermal conductivity ($W/m \times K$)	50
Young's modulus (GPa)	157	Thermal shock resistance ΔT(°C)	600

Source: www.ferrotec.com.tw

2.3 Experimental setup and characteristic measurement

The experimental machine was a micro fine machining center, MEGA III-400, made by ROKU-ROKU, Japan. This machine has the positioning precision of ± 0.0004 mm, axial accuracy of ± 0.0006 mm on Z axis, and repeatability of ± 0.0001 mm. Figure 5 shows the schematic diagram of the force system developed. A triaxial force sensor, 261A01, made by PCB company, U.S.A., was installed on the workpieces side for detecting the force signals. This sensor works by a piezoelectric transducer. Its measuring resolutions of both X and Y axes are 0.0089 N-rms, and that of Z axis is 0.027 N-rms. During the detection, the sampling rate in signal acquisitions was set as 5120 Hz.

Force signals were collected by a data acquisition card of NI 9234 and a compact DAQ (data acquisition) of cDAQ-9171. The analog signals are first transformed to the digital by NI 9234 card and import them into the computer, then the data can be recorded and analyzed by a dynamic signal acquisition software, m + p analyzer v.5.2.1, made by m + p international, Germany. A Bessel low-pass filter was selected to eliminate the high-frequency noises from the captured signals. The maximum filtering frequency was set as 50 Hz.

A working base made of the bakelite was designed on the machine platform for fastening the workpiece and mounting the force sensor under the spindle correctly as shown in Fig. 6. The followed was an acrylic fixture that installed upon the sensor base, and the ceramic workpiece was clipped by four clamps. Two positioning pins of 2-mm diameter were inserted into the acrylic fixture for coupling with the two pin holes on the specified drilling zone, to ensure each trial can be operating over the sensor exactly.

An image measurement instrument, Micro-Vu, Excel-501UC, was used in this study. This device has the positioning precision of 2.5 μm with the reading of 0.1 μm, and the smallest measuring span is 0.25 μm. As a sequence file for setting the measured positions is imported into the system, an Automatic Optical Inspection (**AOI**) process can then be proceeded. Hole characteristics measured in our experiments included the hole diameter, roundness, and positional error.

2.4 Process parameters and experimental plan

In principle, the peck-drilling process of ceramic materials is operated by a higher cutting speed with a lower feed rate. The drilling depth of peck-drilling cycle is another factor affecting chip formations. A two-level through hole experiment, L_8 OA, of a 310-μm diameter was first conducted to investigate the peck-drilling parameters/factors on the thrust force, clarify the interactions between the factors, and derive the correlations between the thrust force and the hole characteristics examined. Table 2 presents the factorial levels of the parameters analyzed. Each factorial level set performed five replicate trials, and every trial drilled 13 through holes on the specified drilling zone as shown in Fig. 3. Thrust forces during the peck-drilling cycles were monitored by the force system and analyzed by the average, standard deviation, and S/N ratio offline.

Secondly, to respond to the application for the spring-load needle used in the wafter testing industry, a three-level stepped hole experiment, L_9 OA, was conducted. Machining of the stepped hole was divided into three procedures: center-pilot hole, upper main hole, and bottom through hole as shown in Fig. 2**(b)**. In addition to the three control factors analyzed in the two-level experiment, the spindle speed for drilling of the bottom through hole was added as a noise factor. Table 3 presents the plan of factorial levels for this experiment.

Table 2
Factorial levels for the two-level through microhole experiment—L_8

Control factor		Level 1	Level 2
A	Cutting speed	7.30 m/min	8.27 m/min
	(Spindle revolution speed)	(7500 rpm))	(8500 rpm)
B	Feed rate	13 mm/min	17 mm/min
C	Depth of peck drilling	0.06 mm	0.08 mm

Table 3
Factorial levels for the three-level stepped microhole experiment—L_9

Control factor		Level 1	Level 2	Level 3
A	Cutting speed (Spindle revolution speed)	8.03 m/min (8250 rpm)	8.27 m/min (8500 rpm)	8.52 m/min (8750 rpm)
B	Feed rate	11 mm/min	13 mm/min	15 mm/min
C	Depth of peck-drilling	0.07 mm	0.08 mm	0.09 mm
N	Spindle speed	9000 rpm	9250 rpm	9500 rpm
N: Noise factor for the drilling of the bottom through hole of Ø156 μm.				

3. Results Of The Two-level Through Microhole Experiment

3.1 Analyses of thrust force

According to the standard two-level L_8 OA, refer **Table A1**, three individual factors are arranged in the columns of 1, 2, and 4, then their interactions can be estimated from the columns of 3, 5, and 6. Because the feed rate and depth of peck-drilling were set as control factors in experiments, the cutting time and number of drilling cycles in the eight trials were dissimilar. Thus, the evaluation of thrust force had some differences. For instance, Fig. 7 shows the force signals of the fifth replica in Trial-6 for drilling a 310-μm-diameter through hole, note as "Trial-6-5". The depth of peck-drilling in Trial-6 was 0.08 mm (level of C2), therefore, it needed 17 cycles to piercing the plate. The feed rate was 13 mm/min (level of B1) so that the time for a peck-drilling cycle in Trial-6 was 0.277 seconds. Accordingly, the total time for drilling a through hole was 4.709 seconds. From the force signals, the peak of thrust force in the first cycle was lower than that of the 2nd to 16th cycles due to parts of material had been removed in the process of center-pilot hole. Regarding the last (17th) cycle, the peak was relatively low, which resulted from the drill had pierced through the bottom surface. Therefore, both the first and last cycles were excluded in the force evaluation; the average of thrust force peaks was calculated based on the data from the 2nd to 16th cycles.

All the averages of thrust force peaks of the central hole (the 7th hole) in the L_8 OA experiment were collected and presented in **Table A1**. For example, in the case of Trial-6-5, the average of thrust force peaks, F_z-5, was 1.030 N, that is the smallest one of the total 40 trials. According to the average values of the five replicas, the mean ($\bar{y}$) and standard deviation (S) were obtained. The signal-to-noise (**S/N**) ratio was calculated by the smaller-the-better equation [23].

$$\mathrm{S/N}_{STB} = -10\log(\bar{y}^{2} + S^{2}) \quad (1)$$

Figure 8 shows the factorial level responses plotted by S/N ratio. The factor affecting the thrust force most greatly was the feed rate (Factor B), the next was the cutting speed (Factor A), and the third was the depth of peck-drilling (Factor C). However, the responses of factorial interactions of A × B, A × C, and B × C were relatively low compared with the individual factors of A, B, and C.

The trials with a larger S/N ratio indicate a better performance based on Taguchi's methods. Both Trial-6 and Trial-5 presented higher S/N ratios, and their means of the averages of thrust force peaks were 1.066 and 1.119 N, respectively. Moreover, from the levels of the cutting speed and feed rate, both trials were identical with A2 and B1, only Factor C was different (**Table A1**). This indicates that while the process is operated by a high-level cutting speed with a low-level feed rate, the thrust force induced is low. The preferred factorial level set was Trial-6 with the factorial levels of A2, B1, and C2.

3.2 Correlations between the thrust force and hole characteristics

For the microhole arrays applied in wafer probe cards, characteristics of the individual microhole affect the functions of microneedles and card's operations, which include the hole diameter, roundness, and positional error. Measurement data of hole characteristics of the central (7th) hole of L_8 OA experiment were summed up and listed in **Table A2.** The S/N ratio of the hole diameter was calculated by the nominal-the-best equation [23]:

$$\mathrm{S/N}_{NTB} = -10\log\left[\left(\bar{y} - m\right)^{2} + S^{2}\right] \quad (2)$$

where m is the target value, 310 μm; and that of the roundness and positional error were calculated as the smaller-the-better case by Eq. (1).

To derive the correlations between the thrust force with different characteristics, normalization treatments of the three characteristics were executed based on their S/N ratios. The value of normalized S/N more approaches to 1 indicates a better achievement. By the same token, the S/N ratios of thrust force of

the eight trials were also normalized. The ranking of the normalized thrust force was Trial-6, Trial-5, Trial-2, Trial-1, Trial-8, Trial-7, Trial-4, and Trial-3, from the large to the small. According to this sequence, relationships between the thrust force and hole characteristics were illustrated as shown in Fig. 9.

From Fig. 9**(a)**, Trial-6 was the best trial in both thrust force and hole diameter. Although Trial-5 was ranked second in the thrust force; however, its normalized S/N in both roundness and positional error was the highest as shown in Fig. 9**(b)** and Fig. 9**(c)**. Observing the linear regression lines of the three figures found that the thrust force presented the most similar trend to the positional error in this experiment.

For a two-level Taguchi's experiment, two conditions of low and high are designated. Factorial ranges and levels for analyzing the responses are limited. A more high-level experiment is still required for parameter optimization to derive available factorial level conditions. From Fig. 8, the level responses of three interactions, A × B, A × C, and B × C, were all lower than that of the individual factors of A, B, and C. This indicates that no evident interactivities found between the factors analyzed on the thrust force. As a result, the fractional-factorial OA can be used in the following three-level stepped microhole experiment confidently.

(a)

4. Results Of The Three-level Stepped Microhole Experiment

Taguchi's L_9 OA was selected in this experiment, which is the most effective OA for the three-level problem considering three control factors. Each factorial level set carried out three replicate trials, and each trial drilled 13 stepped microholes as well. In the same way, the axial thrust force was detected in real-time and three hole characteristics were measured after experiments. From the drilling experience in previous L_8 OA experiment, for reducing the thrust force, levels of the feed rate (Factor B) were decreased slightly, and both cutting speed (Factor A) and depth of peck-drilling (Factor C) were increased contrarily. Factorial levels of the L_9 OA for fractional-factorial experiments are listed in Table 3.

4.1 Analyses of thrust force

As Fig. 2**(b)** shows, after the center-pilot hole, the upper main hole of 310-μm diameter was drilled for a stepped microhole. **Table B1** presents the thrust forces and S/N ratio of the drilling of upper main hole. In the nine trials of L_9 OA, Trial-4 presented the largest S/N ratio of 0.46 dB and the mean of averages of the thrust force peaks was 0.948 N only. On the contrary, the worst one was Trial-6 with the S/N ratio of -2.58 dB; and the mean of averages of the thrust force peaks was increased to 1.345 N.

Figure 10 shows the thrust force signals of the drilling of the 7th holes in Trial-4-1 (the first replica of Trial-4) and Trial-6-1 (the first replica of Trial-6). Both cases experimented by the same cutting speed of A2; however, when the levels of feed rate were specified differently, B1 (Trial-4) and B3 (Trial-6), they resulted in obvious discrepancies. All the thrust force peaks in Trial-6-1 were greater than 1 N (see Fig. 10**(b)**); however, only two peaks were slightly over 1 N in Trial-4-1. Figure 11**(a)** shows the factorial level responses of the thrust force. The feed rate (Factor B) was still the most significant factor; and the preferred factorial level set was A3, B1, and C2.

When the upper main holes were finished, the bottom through holes of 156-μm diameter were drilled. The feed rate and depth of peck-drilling were set constantly as 13 mm/min and 0.03 mm, respectively. Three spindle speeds of 9000, 9250, and 9500 rpm were specified to investigate its influence on the thrust and hole quality. Figure 12 shows the force signals of Trial-7 with different spindle speeds. Their cycle times for the peck-drilling were identical. Each spindle speed had nine trials, and the average of the thrust force peaks are listed in **Table B3**. From the mean and S/N ratio, the high-level spindle speed (9500 rpm) resulted in a lower thrust force.

4.2 Analyses of hole characteristics

Measured data of the hole characteristics of the upper main hole are listed in **Table B2** including hole diameter, roundness, and positional error. Figures 11**(b)-11(d)** show their factorial level responses. Factorial effects for the three characteristics were very dissimilar. The most significant factor of the microhole diameter was the feed rate (Factor B), that of the roundness was the cutting speed (Factor A), and the one for the positional error was the depth of peck-drilling (Factor C). From Taguchi's analyses, the best trial for the microhole diameter was Trial-6 with an average of 309.94 μm, and the best trial for the other two was identical to Trial-1 that had the average roundness of 0.84 μm and positional error of 0.20 μm.

For a stepped microhole matched with the spring-loaded needle (refer Fig. 4), the positional error of the bottom through hole affects the testing position of the microneedle, which needs to be controlled within 3 μm in industry. The measured data and S/N ratio are listed in **Table B3**. The high-level spindle speed (9500 rpm) presented the better performance, and the mean of the averages of positional errors was 0.80 μm only.

4.3 Analysis of variation

Because Taguchi's L_9 OA is a fractional-factorial array, ANOVA analysis must be conducted to estimate whether the experiment succeeded or not and to determine the significances of the factors by using the value of F-test. Table 4 presents the analytical result of ANOVA by the averages of thrust force peaks of the 27 trials (see **Table B1**). When the confidence was set as 95%, both feed rate (Factor B) and depth of peck-drilling (Factor C) were determined as significant factors. The percent contribution of Factor B was high to 77.18%. It was the most significant factor. On the contrary, the cutting speed (Factor A) was the lowest one.

In terms of the error factor, the percent contribution was 12.59% in this analysis. **Ross** [24] pointed out that if the percent contribution due to error (unknown and uncontrolled factors) is low to 15% or less, then it is assumed that no important factors were omitted from the experiment. Therefore, the microdrilling

process were experimented exactly here, and the results of the fractional-factorial L_9 OA were reliable.

Table 4
ANOVA data of the thrust force of drilling the upper main hole in L_9 OA experiment

Control factor	Sum of squares	Degree of freedom	Mean square	F-value	Confidence	Percent contribution (%)	Significance
A	0.009	2	0.004	1.53	75.7%	2.14	No
B	0.314	2	0.157	55.16	100.0%	77.18	Yes
C	0.033	2	0.016	5.77	98.8%	8.08	Yes
Error	0.051	18	0.003			12.59	
Total	0.406	26	Note: At least 95% confidence (F > 3.55)				

4.4 Multi-characteristic analysis

The averages of thrust force peaks of the 40 trials in the two-level L_8 OA experiment were ranged from 1.066 to 1.866 N in the drilling of a 310-μm-diameter hole (refer **Table A1**). After some adjustments in the factorial levels for three-level L_9 OA experiment, the averages of thrust force peaks were dropped to 0.948–1.345 N (refer **Table B1)**.

Although the thrust forces were improved, the significances of the three control factors on the hole characteristics were very different, refer Fig. 11**(b)-(d)**. This study solved this multi-characteristic problem using the Taguchi-based **GRA** method to infer the "optimal parameters level design". The procedures are described as follows [25]:

(1) Normalization of the characteristic values

According to the data of hole characteristics in **Table B2**, normalizations were first conducted to obtain their normalized values for GRA analyses as listed in Table 5. The normalized value more approaches to 1 that indicates a better performance.

(2) Calculation of the grey relational coefficient

In GRA method, a deviation sequence, Δ_{oi}, is obtained by comparing the normalized data of the characteristic with the reference sequence. The grey relational coefficient, $\xi_i(k)$, can then be inferred by Eq. (3).

$$\xi_i(k) = \frac{\Delta_{\min} + \xi \bullet \Delta_{\max}}{\Delta_{oi}(k) + \xi \bullet \Delta_{\max}}$$

3

,

where $\Delta_{oi} = \|x_o(k) - x_i(k)\|$; $x_o(k)$ implies the reference sequence and $x_i(k)$ termed as comparability sequence; $\Delta_{\min}$ and $\Delta_{\max}$ are the minimum and maximum values of the absolute differences (Δ_{oi}); ξ is the distinguishing coefficient which ranges from 0 to 1. The value of ξ was taken as 0.5 here. The data of $\xi_i(k)$ are also presented in Table 5.

(3) Reckoning of the grey relational grade

When the $\xi_i(k)$ is derived, the grey relation grade (**GRG**) of each factorial level set in L_9 OA can be reckoned based on Eq. (4).

$$\gamma_i = \frac{1}{n}\sum_{k=1}^{n} \xi_i(k)$$

4

,

where *n* is the number of response characteristics. The GRG represents the level of correlation between the reference sequence and the comparability sequence and can be the overall representative of all characteristics considered. As a result, the multi-characteristics problem is transferred to a single response problem by GRG. A higher GRG indicates a better performance. In this case, the average GRG of the nine trials was 0.576.

(4) Inference of the optimal parameter level design

Taking the **GRG** as the response, the factorial level responses plot is shown as Fig. 13. The optimal parameters level design was A1, B3, and C1.

Table 5
Grey relational grade calculations for the multi-characteristic analysis

Trial	Control factor			Normalized value			Deviation sequence			Grey relational coef.			Grey relational
	A	B	C	Hole oversize	Roundness	Positional error	Hole oversize	Roundness	Positional error	Hole oversize	Roundness	Positional error	grade (GRG)
Trial-1	1	1	1	0.119	1.000	1.000	0.884	0.000	0.000	0.361	1.000	1.000	0.787
Trial-2	1	2	2	0.476	0.888	0.645	0.524	0.112	0.355	0.488	0.817	0.585	0.630
Trial-3	1	3	3	0.643	0.627	0.203	0.354	0.373	0.797	0.586	0.573	0.386	0.515
Trial-4	2	1	2	0.000	0.065	0.000	1.000	0.935	1.000	0.333	0.349	0.333	0.338
Trial-5	2	2	3	0.310	0.000	0.564	0.695	1.000	0.436	0.418	0.333	0.534	0.429
Trial-6	2	3	1	1.000	0.850	0.235	0.000	0.150	0.765	1.000	0.769	0.395	0.722
Trial-7	3	1	3	0.524	0.763	0.653	0.476	0.237	0.347	0.513	0.678	0.590	0.594
Trial-8	3	2	1	0.286	0.831	0.700	0.713	0.169	0.300	0.412	0.747	0.625	0.595
Trial-9	3	3	2	0.714	0.845	0.045	0.293	0.155	0.955	0.631	0.763	0.344	0.579
Average													0.576

5. Experimental Validations

Two validations were implemented in this study, included the preferred factorial level set of the thrust force derived from L_9 OA experiment and the optimal parameters level design of the multi-characteristic analysis by the **GRG**. Each validation performed three replicate trials.

The validation of the thrust force, Confirm-1, was drilled with the factorial levels of A3, B1, and C2. The mean of the averages of thrust force peaks was 1.023 N as presented in Table 6. For comparison, two cases presented higher S/N ratios in the L_9 OA experiment, L_9 Trial-4 and L_9 Trial-7, are also listed in the table. Confirm-1 and L_9 Trial-4 operated by the same levels of B1 and C2, only the level of Factor A was different. Although the mean of Confirm-1 was higher than L_9 Trial-4, the difference was below 0.1 N. Furthermore, comparing Confirm-1 to L_9 Trial-7, both machined by the same levels of A3 and B1, only the level of Factor C was varied. They also presented a low thrust and had similar statistic values. The thrust forces of the three trials were quite closed. Accordingly, the analytical results were validated.

In terms of the multi-characteristic analysis, the validation (Confirm-2) was drilled with the factorial levels of A1, B3, and C1. Table 7 presents the measured data and statistics of the three characteristics examined. The trials performed well in the L_9 OA experiment are also listed in the right columns. We found that three characteristics in Confirm-2 were all inferior to the best trials in L_9 OA experiment. For instance, the average of the hole diameter was larger than the L_9 Trial-6, which presented a deviation of 1.58 μm from the target value. It may be caused from the drills. Despite both drills used in the L_9 OA experiments and Confirm-2 with the identical nominal dimension, the holes drilled still generated a size deviation due to manufacturing variations. The standard deviation of the hole diameter in Confirm-2 was only 0.096 μm. This indicates that the process was controlled well and satisfied the dimensional specification of 3 μm that the industry required. Regarding the roundness and positional error, the averages were 1.14 μm and 0.18 μm, respectively. Both data showed the process was controlled well and the objective of the multi-characteristic was validated.

Table 6
Experimental validation of the thrust force

Trial	Control factor			Average of thrust force peaks (N)			Mean (N)	Std. dev. (N)	S/N ratio (dB)
	A	B	C	F_z-1	F_z-2	F_z-3			
Confirm-1	3	1	2	1.025	1.054	0.990	1.023	0.032	-0.20
L_9 Trial-4	2	1	2	0.968	0.911	0.965	0.948	0.032	0.46
L_9 Trial-7	3	1	3	0.994	1.022	1.016	1.011	0.015	-0.09

Table 7
Experimental validation of the multi-characteristic analysis

Hole characteristics	Confirm-2 (A1, B3, and C1)					L_9 OA experiment		
	Measured data (μm)			Average (μm)	Std. dev. (μm)	Best trial	Average (μm)	Std. dev. (μm)
	R-1	R-2	R-3					
Hole diameter	311.68	311.59	311.48	311.58	0.096	L_9 Trial-6	309.94	0.092
Roundness	0.96	1.51	0.95	1.14	0.320	L_9 Trial-1	0.84	0.015
Positional error	0.15	0.06	0.33	0.18	0.136	L_9 Trial-1	0.20	0.102

6. Conclusions

This study implemented two series of microdrilling experiments of nitride ceramic plates for checking the interactivity between drilling parameters, minimizing the thrust force, and improving hole characteristics. The stepped microhole drilled was with an upper main hole of 310-μm diameter and a bottom through hole of 156-μm diameter for a spring-loaded microneedle used in the wafer testing industry. From this work, the following points are drawn:

1. From the two-level through microhole experiment (L_8 OA), no evident factorial interactions between the parameters analyzed were found in the thrust force analysis. Drilling by a high-level cutting speed with a low-level feed rate, the thrust force induced is low. In addition, the hole characteristics can be mastered from the real-time thrust force data. In this study, the thrust force presented the most similar trend to the positional error of the microhole drilled.
2. From the three-level stepped microhole experiment (L_9 OA), the lowest thrust force in the drilling of upper main hole was about 1.0 N and that of the bottom through hole was below 0.7 N. Factorial significances for the three hole characteristics examined are very different. The most significant factor of the hole diameter is the feed rate, that of the roundness is the cutting speed, and the one for the positional error is the depth of peck-drilling. This is a multi-characteristic problem.
3. A Taguchi-based GRA model was built to infer the “optimal parameters level design” for the multi-characteristic problem. The parameter levels suggested were drilled by the cutting speed of 8.03 m/min, feed rate of 15 mm/min, and depth of peck-drilling of 0.7 mm.

The drilling parameters derived in this study showed a stable thrust force in the ceramic peck-drilling process and the hole characteristics conformed to the industry requirements. Experimental results provide useful technical data for the process modeling and planning in the drilling of nitride ceramic—Photoveel II.

Declarations

Funding

This work was support by the Ministry of Education, Republic of China (Taiwan) under the project of Interschool Alliance in Teaching on Smart Manufacture Program in 2019 for purchasing the materials and supplies for the experiments.

Consent to participate The authors declare that they all consent to participate this research.

Consent for publication The authors declare that they all consent to publish the manuscript.

Competing interests The authors declare no competing interests.

References

1. Leo Kumar SP, Jerald J, Kumanan S, Prabakaran R (2014) A review on current research aspects in tool-based micromachining processes. Mater Manuf Process 29(11–12):1291–1337. https://doi.org/10.1080/10426914.2014.952037
2. Hyacinth Suganthi X, Natarajan U, Ramasubbu N (2015) A review of accuracy enhancement in microdrilling operations. Int J Adv Manuf Technol 81(1–4):199–217. https://doi.org/10.1007/s00170-015-6900-1
3. Endo H, Marui E (2006) Small-hole drilling in engineering plastics sheet and its accuracy estimation. Int J Machine Tools & Manufacture 46(6):575–579. https://doi.org/10.1177/0954406217742940
4. Patra K, Anand RS, Steiner M, Biermann D (2015) Experimental analysis of cutting forces in microdrilling of austenitic stainless steel (X5CrNi18-10). Mater Manuf Process 30(2):248–255. https://doi.org/10.1080/10426914.2014.941867
5. Anand RS, Patra K, Steiner M, Biermann D (2017) Mechanistic modeling of micro-drilling cutting forces. Int J Adv Manuf Technol 88(1–4):241–254. https://doi.org/10.1007/s00170-016-8632-2
6. Kim DW, Lee YS, Park MS, Chu CN (2009) Tool life improvement by peck drilling and thrust force monitoring during deep-micro-hole drilling of steel. Int J Mach Tools Manuf 49(3–4):246–255. https://doi.org/10.1016/j.ijmachtools.2008.11.005
7. Anand RS, Patra K (2018) Cutting force and hole quality analysis in micro-drilling of CFRP. Mater Manuf Process 33(12):1369–1377. https://doi.org/10.1080/10426914.2017.1401715
8. Rahamathullah I, Shunmugam MS (2012) Analyses of forces and hole quality in micro-drilling of carbon fabric laminate composite. J Compos Mater 47(9):1129–1140. https://doi.org/10.1177/0021998312445594
9. Beruvides G, Quiza R, Rivas M, Castaño F, Haber RE (2014) Online detection of run out in microdrilling of tungsten and titanium alloys. Int J Adv Manuf Technol 74(9–12):1567–1575. https://doi.org/10.1007/s00170-014-6091-1
10. Chang DY, Lin SY (2012) Tool wear, hole characteristics, and manufacturing tolerance in alumina ceramic microdrilling process. Mater Manuf Process 27(3):306–313. https://doi.org/10.1080/10426914.2011.577881
11. Wang C, Cheng K, Rakowski R, Greenwood D, Wale J (2017) Comparative studies on the effect of pilot drillings with application to high-speed drilling of carbon fibre reinforced plastic (CFRP) composites. Int J Adv Manuf Technol 89:3243–3255. https://doi.org/10.1007/s00170-016-9268-y
12. Uysal A (2018) Evaluation of drilling parameters on surface roughness and burr when drilling carbon black reinforce high-density polyethylene. J Compos Mater 52(20):2719–2727. https://doi.org/10.1177/0021998317752505
13. Rajmohan T, Palanikumar K (2011) Optimization of machining parameters for multi-performance characteristics in drilling hybrid metal matrix composites. J Compos Mater 46(7):869–878. https://doi.org/10.1177/0021998311412635
14. Shunmugesh K, Panneerselvam K (2016) Optimization of process parameters in micro-drilling of carbon fiber reinforced Polymer (CFRP) using Taguchi and grey relational analysis. Polym Polym Compos 24(7):499–506. https://doi.org/10.1177/096739111602400708
15. Thanikasalam A, Arunkumar N, Vijayaraj R, Sankaranarayanan V, Senthilkumar E (2019) Online tool condition monitoring and optimizing of process parameters for surface integrity and hole quality in deep hole drilling process. J Balk Tribol Assoc 25(1):1–30. https://scibulcom.net/en/article/ZKSiQSJOdw3wHQmxL8SJ
16. Ravisubramanian S, Shunmugam MS (2018) Investigations into peck drilling process for larger aspect ratio microholes in aluminum 6061-T6. Mater Manuf Process 33(9):935–942. https://doi.org/10.1080/10426914.2017.1376076
17. Wang J, Feng P, Zheng J, Zhang J (2006) Improving hole exit quality in rotary ultrasonic machining of ceramic matrix composites using a compound step-taper drill. Ceram Int 42(12):13387–13394. https://doi.org/10.1016/j.ceramint.2016.05.095
18. Zhang QH, Zhang JH, Sun DM, Zhang QJ, Deng JX (2002) Analysis of fracture at the exit of engineering ceramics during the vibration drilling of a hole. Proc. Inst. Mech. Eng. B. J. Eng. Manuf. 216(8): 1109–1113. https://doi.org/10.1243/095440502760272386
19. Liu JW, Baek DK, Ko TJ (2014) Chipping minimization in drilling ceramic materials with rotary ultrasonic machining. Int J Adv Manuf Technol 72(9–12):1527–1535. https://doi.org/10.1007/s00170-014-5766-y
20. Chang DY, Lin CH (2019) High-aspect ratio mechanical microdrilling process for a microhole array of nitride ceramics. Int J Adv Manuf Technol 100(1–4):2867–2883. https://doi.org/10.1007/s00170-018-2882-0
21. Yaşar N, Günay M, Kılık E, Ünal H (2020) Multiresponse optimization of drillability factors and mechanical properties of chitosan-reinforced polypropylene composite. J Thermoplast Compos Mater. https://doi.org/10.1177/0892705720939163
22. Pervaiz S, Deiab I (2014) Surface roughness and energy consumption analysis of conventional and peck drilling approaches. Proc. Inst. Mech. Eng. B. J. Eng. Manuf. 229(12): 2180–2195. https://doi.org/10.1177/0954405414548464
23. Fowlkes WY, Creveling CM (1984) Engineering methods for robust product design: using Taguchi methods in technology and product development, 1st edn. Addison-Wesley, Massachusetts
24. Ross PJ (1996) Taguchi techniques for quality engineering, 2nd edn. McGraw-Hill, New York
25. Panda A, Sahoo AK, Rout AK (2016) Multi-attribute decision making parametric optimization and modeling in hard turning using ceramic insert through grey relational analysis: a case study. Decis Sci Lett 5(4):581–592. https://doi.org/10.5267/j.dsl.2016.3.001

Figures

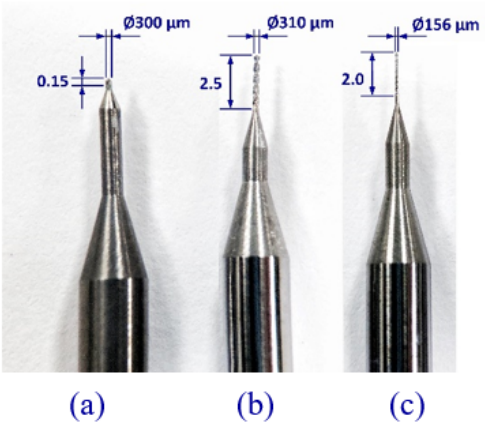

Figure 1

Experimental microdrills: (a) drill for the center-pilot hole, (b) drill for the main hole, and (c) drill for the bottom hole in stepped hole drilling.

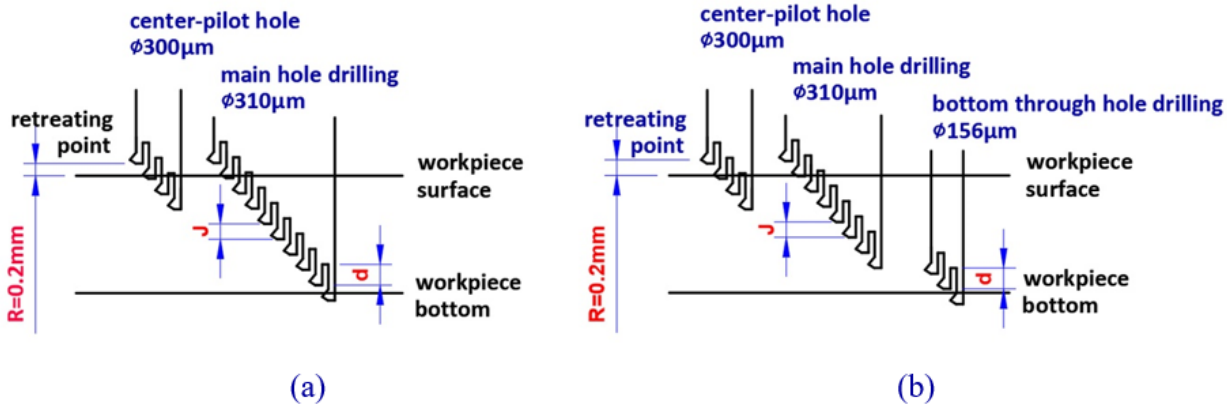

Figure 2

Tool motions in the peck-drilling cycles: (a) two-level through hole experiment and (b) three-level stepped hole experiment

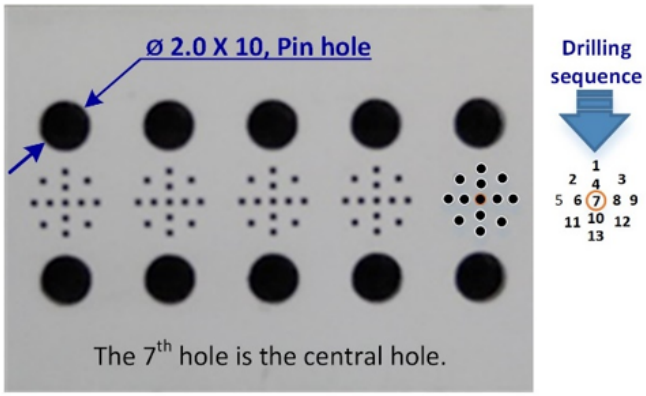

Figure 3

Experimental ceramic plate with five drilling zones

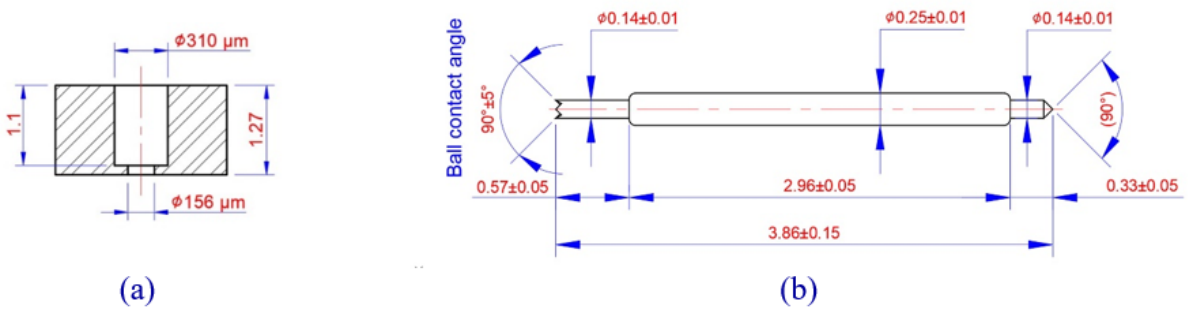

Figure 4

Stepped microhole and its matched microprobe: (a) cross section and (b) spring-loaded microneedle

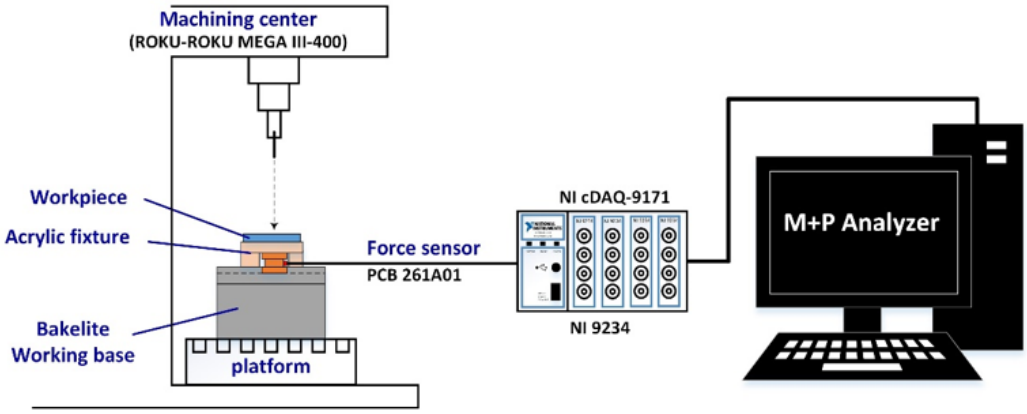

Figure 5

Schematic diagram of the force system

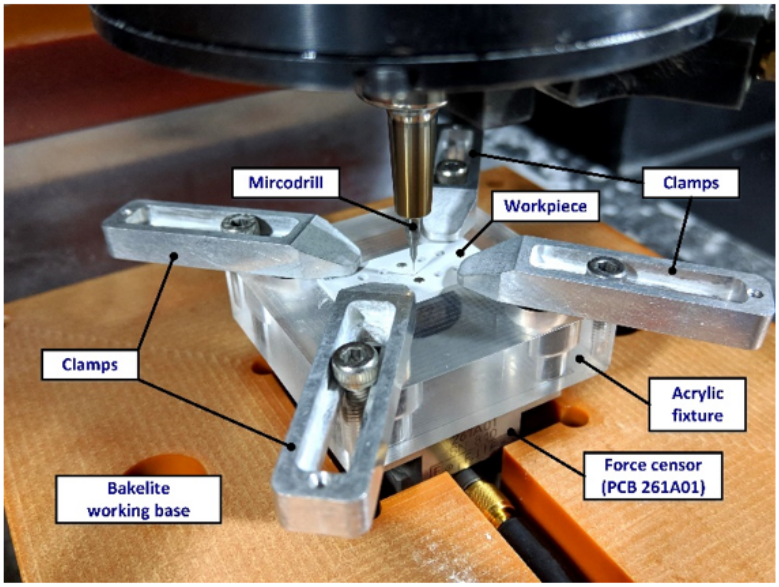

Figure 6

Fixture for fastening the experimental workpiece and force sensor

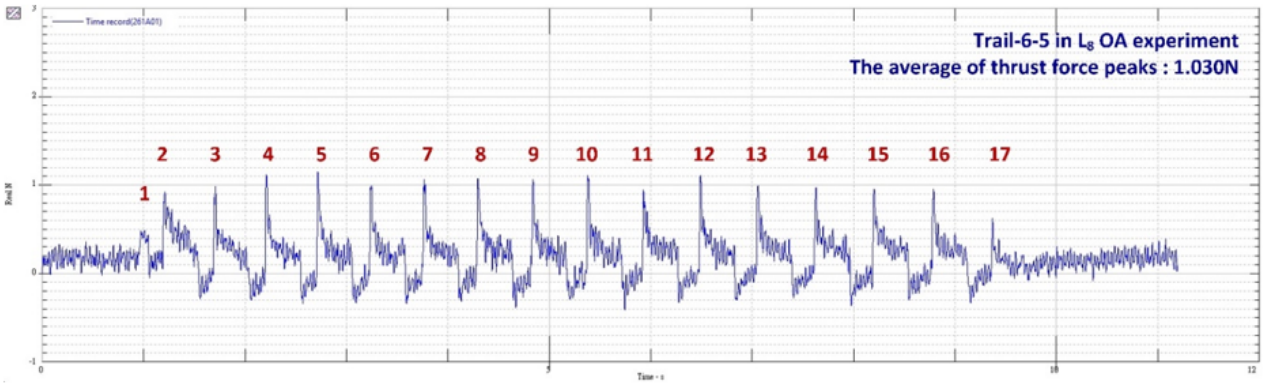

Figure 7

Thrust force signals of Trial-6-5 in L_8 OA through microhole experiment

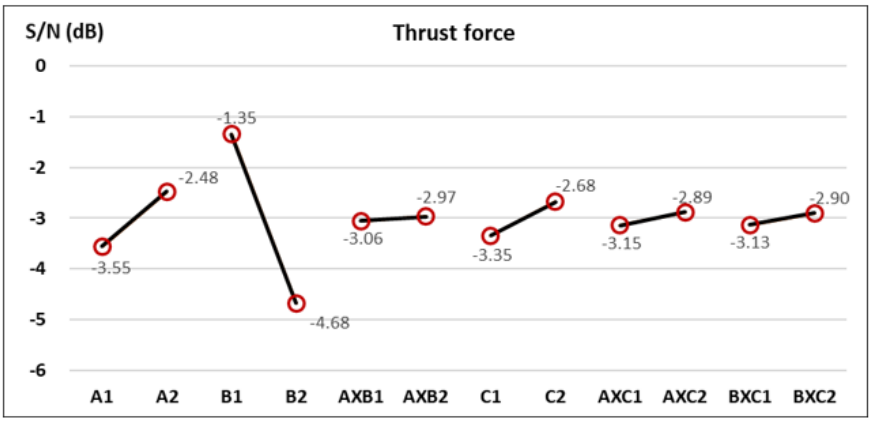

Figure 8

Factorial level responses of the thrust force by S/N ratio in L_8 OA experiment

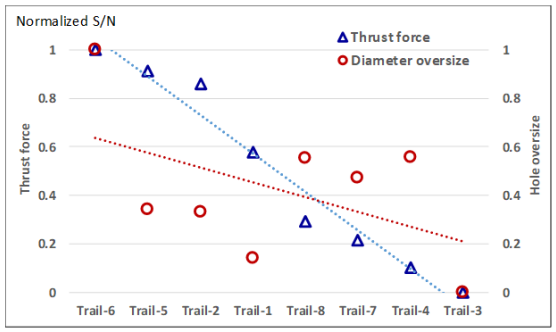

(a)

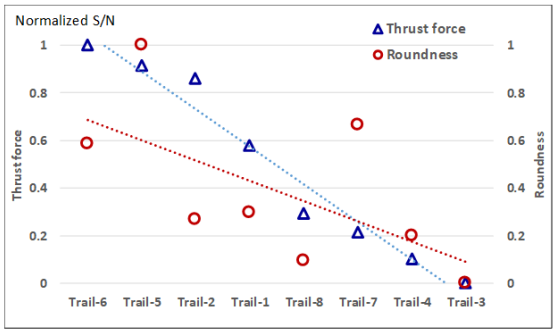

(b)

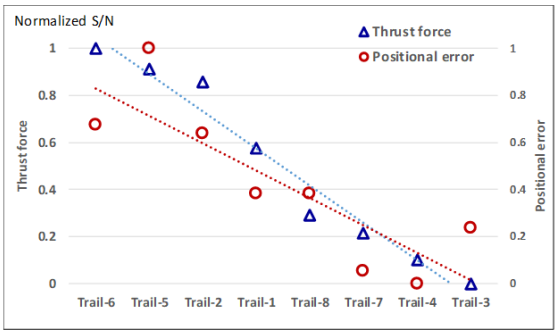

(c)

Figure 9

Relationships between the thrust force and hole characteristics: (a) diameter oversize, (b) roundness, and (c) positional error

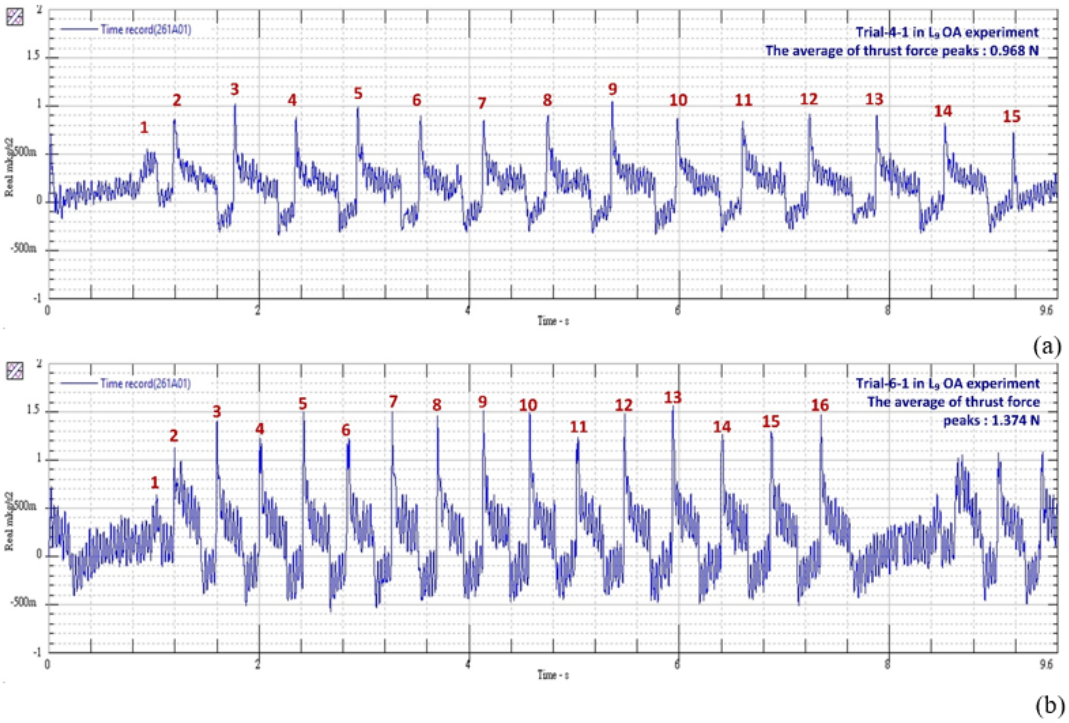

Figure 10

Thrust force signals of the drilling of upper main hole in L_9 OA experiment: (a) Trial-4-1 and (b) Trial-6-1

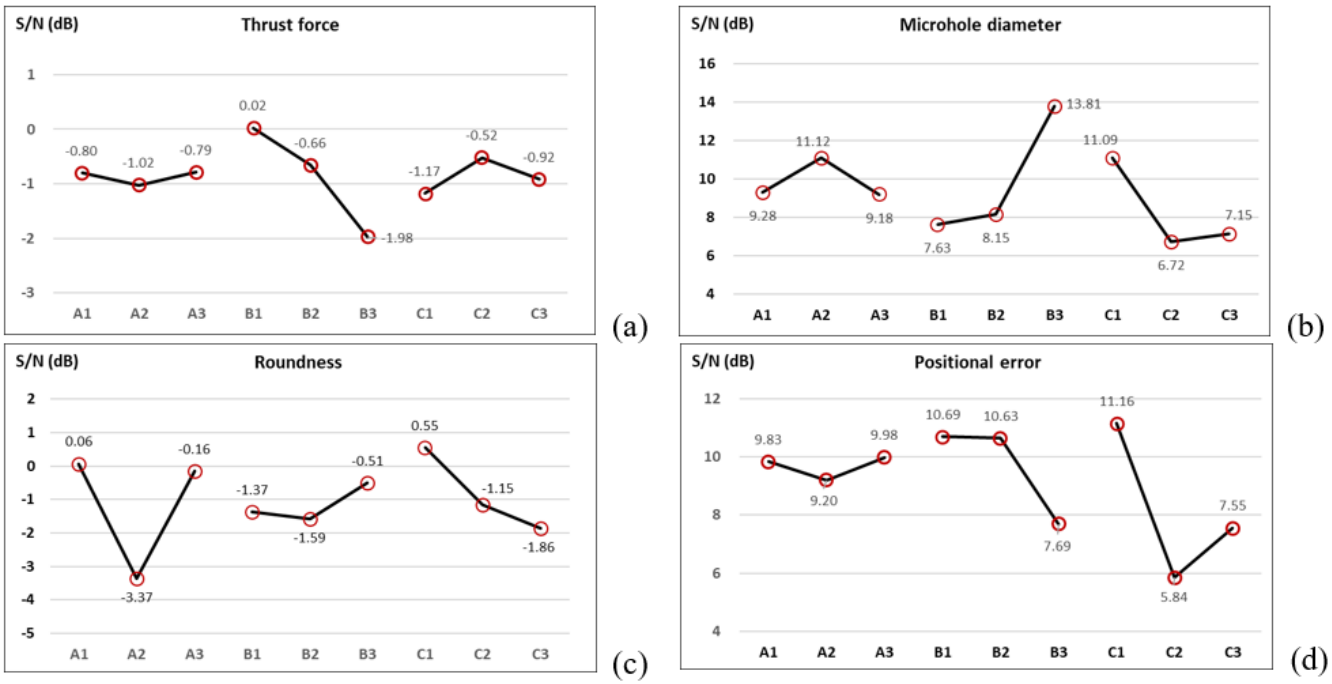

Figure 11

Factorial level responses of the drilling of upper main hole of L_9 OA experiment: (a) thrust force, (b) microhole diameter, (c) roundness, and (d) positional error.

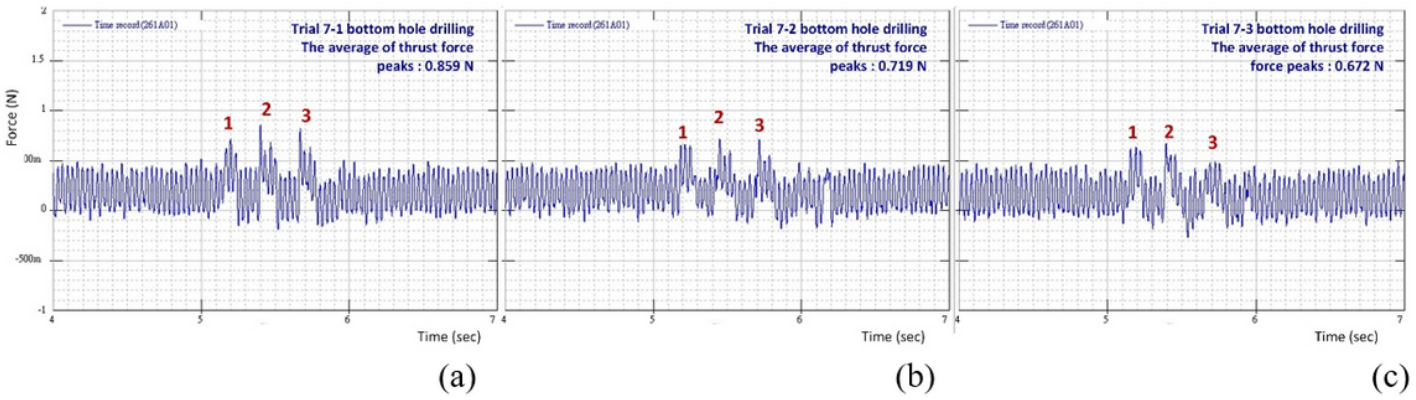

Figure 12

Thrust force signals in the drilling of bottom through hole of Trail-7 of L_9 OA experiment: (a) 9000 rpm, (b) 9250 rpm, and (c) 9500 rpm.

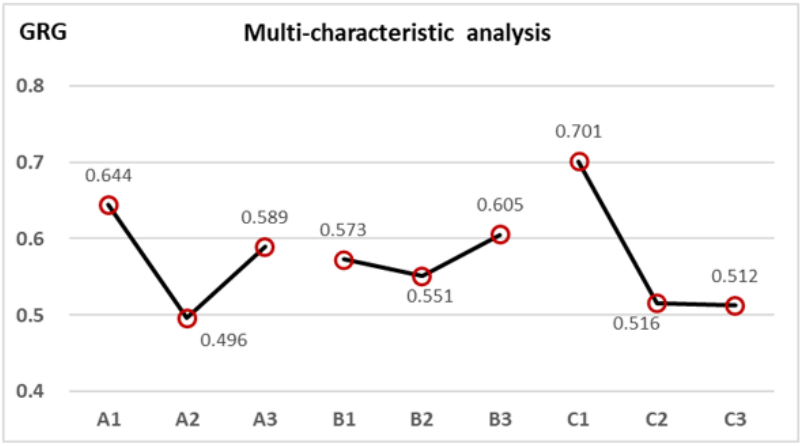

Figure 13

Factorial level responses of the multi-characteristic analysis by GRG

Supplementary Files

This is a list of supplementary files associated with this preprint. Click to download.

- Appendixdata.docx